Studies of the Polarimetric Covariance Matrix. Part I: Calibration Methodology

J. C. HUBBERT, V. N. BRINGI, AND D. BRUNKOW

Colorado State University, Fort Collins, Colorado

(Manuscript received in final form 30 July 2002)

ABSTRACT

A procedure for calibration of the radar covariance matrix for the Colorado State University–University of Chicago–Illinois State Water Survey (CSU–CHILL) radar and S-Band Dual-Polarization Doppler Radar (S-Pol) systems is described. Two relative magnitudes and three offset phases are determined that allow for the calibrated covariance matrix to be constructed. Precise calibration of Z_{dr} is accomplished with use of only sun calibration measurements and crosspolar power measurements from precipitation. No assumptions about the precipitation medium are made. It is also shown how to determine the co-to-cross phase offsets for the CSU–CHILL radar from precipitation data. A novel method for calculating linear depolarization ratio (LDR) that is effective in low signal-to-noise-ratio regions and that requires no knowledge of the background noise temperature is given. This technique utilizes the cross-to-cross covariances. CSU–CHILL data from the Severe Thunderstorm Electrification and Precipitation Study (STEPS) are used to illustrate the LDR estimator and the Z_{dr} calibration technique.

1. Introduction

It is only recently that research weather radars have been configured for measuring the full polarimetric covariance matrix (Bringi and Chandrasekar 2001). Two such radars are the Colorado State University–University of Chicago–Illinois State Water Survey (CSU–CHILL) radar operated by CSU and supported by the National Science Foundation (Brunkow 1999; Brunkow et al. 2000) and the S-Band Dual-Polarization Doppler Radar (S-Pol) operated by the National Center for Atmospheric Research (NCAR) (Keeler et al. 2000), both operating at S-band frequency near 3 GHz. The construction and interpretation of radar covariance matrices has been a recent topic of research, with modeling being the primary focus (Ryzhkov 2001; Hubbert et al. 1999). This paper focuses on a procedure for construction of calibrated covariance matrices. Calibrated covariance matrices have recently been used by Huang et al. (2001) to estimate both mean canting angle and the spread of canting angles of rain drops, and by Hubbert and Bringi (2001) to estimate beam-averaged antenna polarization errors. Even though both radars record all the necessary data for constructing the full covariance matrix, calibration of all the covariances has not been explicitly addressed so far, especially the co-to-cross covariance phases. In this paper only the relative covariance matrix is addressed so that absolute power calibration is not discussed. Our primary focus here to is construct well-calibrated relative covariance matrices to which interesting matrix techniques can be applied (to be addressed in future papers). Absolute power is irrelevant in these techniques. It follows that two relative power terms remain to be calibrated: 1) differential reflectivity (Z_{dr}), and 2) linear depolarization ratio (LDR). Three phase offsets also need to be determined for 1) the copolar differential phase (Ψ_{dp}), 2) the co-to-cross phase ($\arg\{\langle S_{HH}S^*_{VH}\rangle\}$), and 3) the co-to-cross phase ($\arg\{\langle S_{VV}S^*_{HV}\rangle\}$). The accurate estimation of these five terms (two magnitudes and three phases) allows for the construction of calibrated covariance matrices. This paper then shows specifically how to determine these five calibration quantities for both the CSU–CHILL radar and S-Pol.

A novel method to calibrate Z_{dr} is given that depends only on a sun calibration measurement and the difference of the two crosspolar powers obtained from precipitation. This solution is analytical and requires no assumptions other than reciprocity. A more established method to determine the Z_{dr} system offset uses vertical pointing data in precipitation where it is assumed that Z_{dr} is 0 dB when data are averaged over a full 360° rotation of the antenna (Bringi and Chandrasekar 2001; Gorgucci et al. 1999). No such assumptions are necessary with the method presented here.

Finally, a novel technique for the estimation of LDR is given that utilizes the cross-to-cross covariance. This technique is immune to background noise and thus no knowledge of the noise temperature is needed for noise correction, which makes the technique attractive for low signal-to-noise ratio (SNR) regions. Radar data from the

Corresponding author address: Dr. J. C. Hubbert, NCAR/ATD, PO Box 3000, Boulder, CO 80307.
E-mail: hubbert@ucar.edu

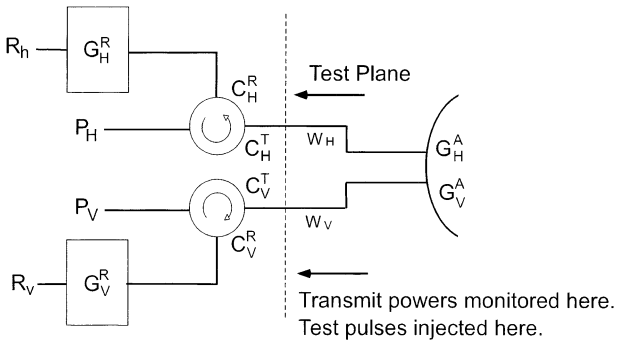

FIG. 1. Block diagram of the CSU–CHILL radar: $P_{H,V}$ are the input transmitter powers, C refers to the circulator insertion loss, W is the waveguide loss, $G^A_{H,V}$ are the antenna gains, $G^R_{H,V}$ are the receiver gains, and $R_{H,V}$ are the signal powers at the receiver outputs.

Severe Thunderstorms Electrification and Precipitation Study (STEPS) field campaign are used to illustrate the LDR estimation technique and Z_{dr} calibration technique.

2. Theory

a. CSU–CHILL radar

The CSU–CHILL radar uses two separate transmitters and two receivers for measuring the polarimetric covariance matrix (Brunkow et al. 2000). Shown in Fig. 1 is a simplified block diagram of the CSU–CHILL radar, where $P_{H,V}$ are the input transmitter powers, $C^T_{H,V}$ are the losses associated with the circulators on transmission, $C^R_{H,V}$ are the losses associated with the circulators on reception, $W_{H,V}$ are waveguide losses, $G^A_{H,V}$ are the antenna gains, $G^R_{H,V}$ are the receiver gains, and $R_{H,V}$ are the received powers. The dotted line represents the measurement plane where both the transmit power is monitored and test signals are injected. From Fig. 1 it follows that

$$Z^m_{dr} = \frac{P_H C^T_H W^2_H (G^A_H)^2 C^R_H G^R_H \langle |S_{HH}|^2 \rangle}{P_V C^T_V W^2_V (G^A_V)^2 C^R_V G^R_V \langle |S_{VV}|^2 \rangle}, \quad (1)$$

$$\mathrm{LDR}^m_H = \frac{W_V G^A_V C^R_V G^R_V \langle |S_{VH}|^2 \rangle}{W_H G^A_H C^R_H G^R_H \langle |S_{HH}|^2 \rangle}, \quad (2)$$

where Z^m_{dr} and LDR^m_H are measured differential reflectivity and linear depolarization ratio, respectively. Note that $\langle |S_{HH}|^2 \rangle / \langle |S_{VV}|^2 \rangle = Z_{dr}$ and $\langle |S_{VH}|^2 \rangle / \langle |S_{HH}|^2 \rangle = \mathrm{LDR}_H$ are the intrinsic values we wish to isolate, with $\langle * \rangle$ denoting time average. Available for calibration are sun calibration measurements ($\mathcal{S}$), a test pulse measurement ($\mathcal{T}$), and a transmit power measurement ($\mathcal{Q}$) defined as

$$\mathcal{S} = \frac{W_V G^A_V C^R_V G^R_V}{W_H G^A_H C^R_H G^R_H}, \quad (3)$$

$$\mathcal{T} = \frac{C^R_V G^R_V}{C^R_H G^R_H}, \quad (4)$$

$$\mathcal{Q} = \frac{P_H C^T_H}{P_V C^T_V}. \quad (5)$$

The differential gain of the two receive paths is measured by pointing the radar at the sun through a precipitation-free region (the H and V powers radiated from the sun are considered equal, i.e., unpolarized). Also, a test pulse is injected at the test plane (equal amplitude in both channels) in order to track the temporal variation of the differential gain of the receive path circulators and the receivers. The transmit powers are monitored at the test plane in order to determine the differential transmit power. From (1)–(5),

$$Z_{dr} = Z^m_{dr} \frac{\mathcal{S}^2}{\mathcal{Q}\mathcal{T}}, \quad (6)$$

$$\mathrm{LDR}_H = \mathrm{LDR}^m_H \frac{1}{\mathcal{S}}. \quad (7)$$

Though not shown explicitly, $\mathrm{LDR}_V = \mathrm{LDR}^m_V \mathcal{S}$ where $\mathrm{LDR}_V = \langle |S_{HV}|^2 \rangle / \langle |S_{VV}|^2 \rangle$. If $\mathcal{S}$, $\mathcal{T}$, and $\mathcal{Q}$ are all accurately monitored, then Z_{dr} and LDR can be determined quite accurately. However, in practice, there are errors associated with these measurements that can bias Z_{dr}. These errors can be eliminated if the crosspolar powers are utilized. The ratio of the two received crosspolar power is

$$\frac{R_{VHVH}}{R_{HVHV}} = \frac{P_H C^T_H C^R_V G^R_V \langle |S_{VH}|^2 \rangle}{P_V C^T_V C^R_H G^R_H \langle |S_{HV}|^2 \rangle}. \quad (8)$$

Because of reciprocity (Saxon 1955), $\langle |S_{VH}|^2 \rangle = \langle |S_{HV}|^2 \rangle$, and it follows that

$$Z_{dr} = Z^m_{dr} \mathcal{S}^2 \frac{R_{HVHV}}{R_{VHVH}}. \quad (9)$$

This equation is important in that Z^m_{dr} can be calibrated using only sun calibration data plus precipitation data: no power meters or other monitoring is needed. Furthermore, the process can be automated. The only requirement is that the sun calibration needs to be repeated with a frequency dictated by the stability of the differential gain of the receive path of the radar system. Note that even the transmit power need not be monitored. Typically, Z_{dr} is calibrated via vertical pointing data in precipitation, which relies upon the assumption that the average Z_{dr} is intrinsically zero for hydrometeors at vertical incidence when the polarization basis is rotated 360° in azimuth. This indeed should be true; however, it is evident from examining vertical pointing data from several radars around the world that other scattering mechanisms can be present other than direct scatter from the precipitation in the main beam of the radar. It is known that vertically pointing Z_{dr} can be a function of azimuth angle (Gorgucci et al. 1999; Bringi and Chandrasekar 2001), having sinusoidal-like variations with peak-to-peak excursions of several tenths of a decibel. This behavior has been surmised to be caused by antenna pattern sidelobes interacting with ground clutter. For the CSU–CHILL radar, these sinusoidal-like variations are observed but are not always present. Fur-

thermore, these variations are not observed in clear air. If ground clutter were responsible, then these sinusoidal-like variations would be seen even when vertical pointing data are taken in clear air. We speculate that back lobes of the antenna pattern interact with the precipitation medium via multipath scattering to cause the azimuthal variation. If this is true, then Z_{dr} from this multipath scatter will not necessarily give 0 dB when Z_{dr} is integrated over 360° since the ground scatter cross sections will not be the same for H and V polarizations. It is also possible that the azimuthal variation of Z_{dr} is an artifact of a wet radome or due to imperfections in the isolation of the dual-channel rotary joint with azimuth angle (though this proved not to be the case for the CSU–CHILL radar). Other practical problems with vertical pointing data are infrequent occurrence of precipitation over the radar and the minimum range needed to be in the far field ($2D^2/\lambda$, where D is the antenna diameter and λ is the wavelength). The procedure based on (9) offers significant advantages since crosspolar power will routinely be available from precipitation. Furthermore, ground clutter targets should also obey reciprocity so that ground clutter data can also be used. Since the ratio of R_{HVHV} and R_{VHVH} represents a system bias that should be constant over 5–10-min intervals, this ratio can be more accurately estimated by averaging over an entire volume of precipitation. Examples are given in section 3, ''Data analysis.''

1) PHASE CALIBRATION

First, six phase terms are defined:

$\phi_{Ht} \equiv$ phase of the H transmit wave at the antenna H port,

$\phi_{Vt} \equiv$ phase of the V transmit wave at the antenna V port,

$\phi_{Hr} \equiv$ phase shift due to the total H receive path,

$\phi_{Vr} \equiv$ phase shift due to the total V receive path,

vel $\equiv$ Doppler phase proportional to the mean velocity of the scatterers within the resolution volume,

$\Psi_{dp} \equiv$ total copolar differential phase (due to both forward scatter and backscatter). (10)

Figure 2 illustrates the four time series measured by the radar represented as HH_i, VV_i, VH_i, and HV_i, with the V-polarized pulse being transmitted first. It is easy to show that (Sachidananda and Zrnić 1986; Mueller 1984)

$$\mathcal{A} = \arg\langle VV_i^* HH_i\rangle = \text{vel} - \Psi_{dp} + (\phi_{Ht} - \phi_{Vt}) + (\phi_{Hr} - \phi_{Vr}), \quad (11)$$

$$\mathcal{B} = \arg\langle VV_{i+1} HH_i^*\rangle = \text{vel} + \Psi_{dp} - (\phi_{Ht} - \phi_{Vt}) - (\phi_{Hr} - \phi_{Vr}), \quad (12)$$

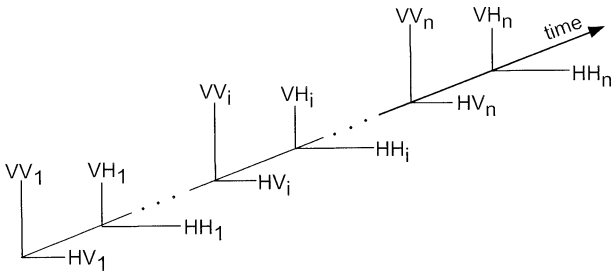

FIG. 2. Time series schematic of the received signals for a dual-polarized radar. Numeric subscripts refer to the pulse number (ordered in pairs): e.g., notation VH refers to H transmit and V receive.

$$\mathcal{C} = \arg\langle HV_i^* VH_i\rangle = \text{vel} + (\phi_{Ht} - \phi_{Vt}) - (\phi_{Hr} - \phi_{Vr}), \quad (13)$$

$$\mathcal{D} = \arg\langle HV_{i+1} VH_i^*\rangle = \text{vel} - (\phi_{Ht} - \phi_{Vt}) + (\phi_{Hr} - \phi_{Vr}). \quad (14)$$

Combining these equations gives

$$(\mathcal{A} - \mathcal{B} + \mathcal{C} - \mathcal{D})/2 = -\Psi_{dp} + 2(\phi_{Ht} - \phi_{Vt}), \quad (15)$$

$$(\mathcal{A} - \mathcal{B} - \mathcal{C} + \mathcal{D})/2 = -\Psi_{dp} + 2(\phi_{Hr} - \phi_{Vr}). \quad (16)$$

Equations (15) and (16) are interesting because they show that not only the receive phase difference, $\phi_{Hr} - \phi_{Vr}$, but also the transmit phase difference, $\phi_{Ht} - \phi_{Vt}$, can be determined solely from precipitation measurements. Unfortunately, neither the CSU–CHILL radar nor S-Pol routinely record the cross-to-cross covariances, $\langle HV_i^* VH_i\rangle$ and $\langle HV_i VH_i^*\rangle$; however, CSU–CHILL does periodically gather time series data from which all covariances are available. To eliminate Ψ_{dp} from (15) and (16) either data can be selected from ranges where insignificant Ψ_{dp} has accumulated, or, alternately, Ψ_{dp} can be be estimated and removed. The receive phase difference can also be determined from sphere calibration or remote horn measurements, but the convenience of determining these phase offsets, which may vary on a day-to-day basis, from precipitation data is obvious. To find the Ψ_{dp} offset, Ψ_{dp_off}, $\mathcal{A}$ and $\mathcal{B}$ are combined as follows:

$$\frac{\mathcal{B} - \mathcal{A}}{2} = \Psi_{dp} - (\phi_{Ht} - \phi_{Vt}) - (\phi_{Hr} - \phi_{Vr}), \quad (17)$$

which is how Ψ_{dp} is typically calculated (Mueller 1984). Since the intrinsic range profiles of Ψ_{dp} should begin at 0°, $\Psi_{dp\_off} = -(\phi_{Ht} - \phi_{Vt}) - (\phi_{Hr} - \phi_{Vr})$ can be easily found from range profiles of $(\mathcal{B} - \mathcal{A})/2$.

Next the phase offsets of the co-to-cross covariances are determined. The phases for the two co-to-cross covariances can be written as

$$\mathcal{E} = \arg\{\langle VH_i HH_i^*\rangle\} = \theta_H - (\phi_{Hr} - \phi_{Vr}), \quad (18)$$

$$\mathcal{F} = \arg\{\langle VV_i HV_i^*\rangle\} = \theta_V - (\phi_{Hr} - \phi_{Vr}), \quad (19)$$

where $\theta_{H,V}$ represent the intrinsic co-to-cross covariance

phases (Hubbert et al. 1999). If the cross-to-cross covariances are available, (16) can be used to determine the offset phase, $\phi_{Hr} - \phi_{Vr}$, but this offset can also be found as follows. It is known that $\theta_H + \theta_V = \Psi_{dp}$ (Jameson 1985; Hubbert et al. 1999), so that

$$\mathcal{E} + \mathcal{F} = \Psi_{dp} - 2(\phi_{Hr} - \phi_{Vr}). \quad (20)$$

Since $\mathcal{E}$ and $\mathcal{F}$ contain the identical offset phase term, (20) suggests an alternate way to estimate the phase offset term $\phi_{Hr} - \phi_{Vr}$. A constant phase can be added to both $\mathcal{E}$ and $\mathcal{F}$ and be adjusted until a range profile of $\mathcal{E} + \mathcal{F}$ lies upon the offset-corrected Ψ_{dp} range profile. Since range profiles of $\mathcal{E} + \mathcal{F}$ typically have high variance, the range profiles should first be filtered (similar to filtering Ψ_{dp} for calculating K_{dp}, specific differential phase; Hubbert and Bringi 1995). This technique works best when there is a significant amount of Ψ_{dp} accumulation (e.g., propagation path through intense multiple rain cells), and it is attractive since it is based on data alone. The reason for this is that in regions of large Ψ_{dp} accumulation, the SNR is typically large and data quality is high.

Having now determined the two magnitude calibration terms and the three phase offset terms, the calibrated covariance matrix can be constructed. First, the following variables are defined:

$$P_H = \langle |HH_i|^2 \rangle \quad \text{H power (used as a reference)},$$

$$P_V = P_H \frac{1}{Z_{dr}} \quad \text{calibrated V power},$$

$$P_{xH} = \mathrm{LDR}_H^m \frac{1}{S} P_H \quad \text{calibrated cross power (H transmit)},$$

$$P_{xV} = \mathrm{LDR}_V^m S P_V \quad \text{calibrated cross power (V transmit)},$$

$$\rho_{xH} = \frac{\langle HH_i VH_i^* \rangle}{[\langle |HH_i|^2 \rangle \langle |VH_i|^2 \rangle]^{0.5}} \quad \text{co-to-cross correlation coefficient},$$

$$\rho_{xV} = \frac{\langle VV_i HV_i^* \rangle}{[\langle |VV_i|^2 \rangle \langle |HV_i|^2 \rangle]^{0.5}} \quad \text{co-to-cross correlation coefficient},$$

$$\rho_{HV} = \frac{0.5(|\langle VV_i^* HH_i \rangle| + |\langle VV_{i+1} HH_i^* \rangle|) \exp^{j\Psi_{dp}^m}}{[\langle |HH_i|^2 \rangle \langle |VV_i|^2 \rangle]^{0.5} \rho_{HH}(2)^{0.25}} \quad \text{copolar correlation coefficient}, \quad (21)$$

where

$$\rho_{HH}(2) = \frac{|\langle HH_i HH_{i+1} \rangle|}{\langle |HH_i|^2 \rangle}, \quad (22)$$

$$\Psi_{dp}^m = \arg\{\langle VV_{i+1} HH_i^* \rangle \langle VV_i HH_i^* \rangle\}/2. \quad (23)$$

The calibrated covariance matrix is then defined as

$$\begin{bmatrix} P_H & \sqrt{2}\rho_{xH}(P_H P_{xH})^{0.5} \exp^{(-j\phi_{x\_off})} & \rho_{HV}^*(P_H P_V)^{0.5} \exp^{(j\phi_{dp\_off})} \\ \sqrt{2}\rho_{xH}^*(P_H P_{xH})^{0.5} \exp^{(j\phi_{x\_off})} & P_{xH} + P_{xV} & \sqrt{2}\rho_{xV}^*(P_V P_{xV})^{0.5} \exp^{(-j\phi_{x\_off})} \\ \rho_{HV}(P_V P_H)^{0.5} \exp^{(-j\phi_{dp\_off})} & \sqrt{2}\rho_{xV}(P_V P_{xV})^{0.5} \exp^{(j\phi_{x\_off})} & P_V \end{bmatrix}, \quad (24)$$

where $\phi_{x\_off} = \phi_{Hr} - \phi_{Vr}$ and $\Psi_{dp\_off} = -(\phi_{Ht} - \phi_{Vt}) - \phi_{x\_off}$. [See Tragl (1990) for covariance matrix background.]

b. S-Pol

S-Pol uses a single transmitter and a mechanical polarization switch to transmit alternate pulses of H and V polarization. Two receivers are used to measure the copolar and crosspolar return signals. The S-Pol system block diagram is similar to the CSU–CHILL block diagram (Fig. 1) except that there is a transfer switch in the receiver path after the circulators, as shown in Fig. 3. The switch allows for the H and V incoming signals to be directed to either the co- or cross receiver. The object of this arrangement is to reduce the measurement bias of Z_{dr} that can be caused by using two separate receivers that may not be perfectly matched in gain over the entire dynamic range. Because of the transfer switch, the analysis is slightly more complicated. Since there are four possible paths through the receiver chain, four sun calibration numbers are required (see the appendix). It can be shown that for the S-Pol configuration,

$$Z_{dr}^m = \frac{P_H C_H^T W_H^2 (G_H^A)^2 C_H^R \Gamma_{co,H} \langle |S_{HH}|^2 \rangle}{P_V C_V^T W_V^2 (G_V^A)^2 C_V^R \Gamma_{co,V} \langle |S_{VV}|^2 \rangle}, \quad (25)$$

$$\mathrm{LDR}_H^m = \frac{W_V G_V^A C_V^R \Gamma_{x,V} G_x^R \langle |S_{VH}|^2 \rangle}{W_H G_H^A C_H^R \Gamma_{co,H} G_{co}^R \langle |S_{HH}|^2 \rangle}, \quad (26)$$

where $\Gamma_{co,V}$, $\Gamma_{co,H}$, and $\Gamma_{x,V}$ represent the insertion losses associated with various paths through the switch. For example, $\Gamma_{co,V}$ represents the path from the V switch input through the switch to the copolar receiver. The ratio of the crosspolar powers becomes

$$\frac{R_{VHVH}}{R_{HVHV}} = \frac{P_H C_H^T C_V^R \Gamma_{x,V} \langle |S_{VH}|^2 \rangle}{P_V C_V^T C_H^R \Gamma_{x,H} \langle |S_{HV}|^2 \rangle}. \quad (27)$$

The difference between (27) and (8) is that (8) contains the ratio of the two receiver gains, whereas (27) contains a ratio of insertion loss due to receive paths through the switch. For the S-Pol configuration, Z_{dr}^m and LDR_H^m can be calibrated similar to (9) and (7):

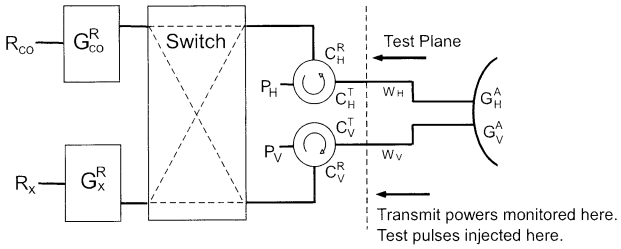

FIG. 3. Block diagram of part of the S-Pol receiver section. The H and V signals can be directed to either the co- or cross receiver (see also Fig. 1). The mechanical switch is not shown.

$$\mathrm{LDR}_\mathrm{H} = \mathrm{LDR}_\mathrm{H}^m \frac{1}{\mathcal{S}_3}, \tag{28}$$

$$Z_\mathrm{dr} = Z_\mathrm{dr}^m \mathcal{S}_1 \left(\mathcal{S}_2 \frac{R_\mathrm{HVHV}}{R_\mathrm{VHVH}} \right), \tag{29}$$

where $\mathcal{S}_1$, $\mathcal{S}_2$, and $\mathcal{S}_3$ are as defined in the appendix.

S-POL PHASE CALIBRATION

Phase calibration is more complicated for S-Pol than for CSU–CHILL due to the transfer switch in the receiver configuration. First phases for the receiver paths are defined as follows.

$\beta_\mathrm{Hr} \equiv$ phase shift due to the H receive path up to the switch,

$\beta_\mathrm{Vr} \equiv$ phase shift due to the V receive path up to the switch,

$\alpha_\mathrm{co,H} \equiv$ phase shift from the H input port of the switch to the coreceiver,

$\alpha_{x,\mathrm{H}} \equiv$ phase shift from the H input port of the switch to the cross-receiver,

$\alpha_\mathrm{co,V} \equiv$ phase shift from the V input port of the switch to the coreceiver,

$\alpha_{x,\mathrm{V}} \equiv$ phase shift from the V input port of the switch to the cross-receiver,

$\phi_{G_\mathrm{co}^R} \equiv$ phase shift due to the coreceiver,

$\phi_{G_x^R} \equiv$ phase shift due to the cross-receiver. (30)

Analogous to (11)–(14), it is straightforward to show that

$$\begin{aligned} \mathcal{A} &= \arg\langle \mathrm{VV}_i^* \mathrm{HH}_i \rangle \\ &= \mathrm{vel} - \Psi_\mathrm{dp} + (\phi_\mathrm{Ht} - \phi_\mathrm{Vt}) + (\beta_\mathrm{Hr} - \beta_\mathrm{Vr}) \\ &\quad + (\alpha_\mathrm{co,H} - \alpha_\mathrm{co,V}), \end{aligned} \tag{31}$$

$$\begin{aligned} \mathcal{B} &= \arg\langle \mathrm{VV}_{i+1} \mathrm{HH}_i^* \rangle \\ &= \mathrm{vel} + \Psi_\mathrm{dp} - (\phi_\mathrm{Ht} - \phi_\mathrm{Vt}) - (\beta_\mathrm{Hr} - \beta_\mathrm{Vr}) \\ &\quad - (\alpha_\mathrm{co,H} - \alpha_\mathrm{co,V}), \end{aligned} \tag{32}$$

$$\begin{aligned} \mathcal{C} &= \arg\langle \mathrm{HV}_i^* \mathrm{VH}_i \rangle \\ &= \mathrm{vel} + (\phi_\mathrm{Ht} - \phi_\mathrm{Vt}) - (\beta_\mathrm{Hr} - \beta_\mathrm{Vr}) \\ &\quad + (\alpha_{x,\mathrm{H}} - \alpha_{x,\mathrm{V}}), \end{aligned} \tag{33}$$

$$\begin{aligned} \mathcal{D} &= \arg\langle \mathrm{HV}_{i+1} \mathrm{VH}_i^* \rangle \\ &= \mathrm{vel} - (\phi_\mathrm{Ht} - \phi_\mathrm{Vt}) + (\beta_\mathrm{Hr} - \beta_\mathrm{Vr}) \\ &\quad - (\alpha_{x,\mathrm{H}} - \alpha_{x,\mathrm{V}}). \end{aligned} \tag{34}$$

For S-Pol, $\Psi_\mathrm{dp\_off} = -(\phi_\mathrm{Ht} - \phi_\mathrm{Vt}) - (\beta_\mathrm{Hr} - \beta_\mathrm{Vr}) - (\alpha_\mathrm{co,H} - \alpha_\mathrm{co,V})$ and again can be determined by forcing range profiles of $(\mathcal{B} - \mathcal{A})/2$ to begin at 0°. As was done for CSU–CHILL analysis, the above phases can be combined:

$$\begin{aligned} &(\mathcal{A} - \mathcal{B} + \mathcal{C} - \mathcal{D})/2 \\ &\quad = -\Psi_\mathrm{dp} + 2(\phi_\mathrm{Ht} - \phi_\mathrm{Vt}) + (\alpha_\mathrm{co,H} - \alpha_\mathrm{co,V}) \\ &\qquad - (\alpha_{x,\mathrm{H}} - \alpha_{x,\mathrm{V}}), \end{aligned} \tag{35}$$

$$\begin{aligned} &(\mathcal{A} - \mathcal{B} - \mathcal{C} + \mathcal{D})/2 \\ &\quad = -\Psi_\mathrm{dp} + 2(\beta_\mathrm{Hr} - \beta_\mathrm{Vr}) + (\alpha_\mathrm{co,H} - \alpha_\mathrm{co,V}) \\ &\qquad + (\alpha_{x,\mathrm{H}} - \alpha_{x,\mathrm{V}}). \end{aligned} \tag{36}$$

As can be seen, the differential transmit path phase and the differential receive path phases are not conveniently separated here as was the case in (15) and (16). The co-to-cross phases for the S-Pol configuration are

$$\begin{aligned} \mathcal{E} &= \arg\{\langle \mathrm{VH}_i \mathrm{HH}_i^* \rangle\} \\ &= \theta_\mathrm{H} - (\beta_\mathrm{Hr} - \beta_\mathrm{Vr}) + (\alpha_{x,\mathrm{V}} - \alpha_\mathrm{co,H}) - (\phi_{G_\mathrm{co}^R} - \phi_{G_x^R}), \end{aligned} \tag{37}$$

$$\begin{aligned} \mathcal{F} &= \arg\{\langle \mathrm{VV}_i \mathrm{HV}_i^* \rangle\} \\ &= \theta_\mathrm{V} - (\beta_\mathrm{Hr} - \beta_\mathrm{Vr}) + (\alpha_\mathrm{co,V} - \alpha_{x,\mathrm{H}}) + (\phi_{G_\mathrm{co}^R} - \phi_{G_x^R}), \end{aligned} \tag{38}$$

and summing gives

$$\begin{aligned} \mathcal{E} + \mathcal{F} &= \Psi_\mathrm{dp} - 2(\beta_\mathrm{Hr} - \beta_\mathrm{Vr}) + \alpha_\mathrm{co,V} - \alpha_\mathrm{co,H} \\ &\quad + \alpha_{x,\mathrm{V}} - \alpha_{x,\mathrm{H}}. \end{aligned} \tag{39}$$

As was done with CSU–CHILL analysis, the phase offset term in (39), $-2(\beta_\mathrm{Hr} - \beta_\mathrm{Vr} + \alpha_\mathrm{co,V} - \alpha_\mathrm{co,H} + \alpha_{x,\mathrm{V}} - \alpha_{x,\mathrm{H}}$, can be determined by finding the phase constant that will make range profiles of $\mathcal{E} + \mathcal{F}$ begin at 0° (or by comparing to a range profiles of Ψ_dp). However, this phase offset is not the phase offset required in (37) and (38). As can be seen from (37) and (38), the phase difference of the two receivers, $\phi_{G_\mathrm{co}^R} - \phi_{G_x^R}$, is present but is absent from all the other phase equations. Therefore, it is impossible to determine the phase offsets of the co-to-cross covariances from precipitation measurements for the S-Pol system configuration with the covariances considered here. One way to determine the phase offsets in (37) and (38) is to transmit with a remote linear test horn at a 45° tilt angle and then measure the

S-Pol receiver phase differences. Such test data, though currently unavailable, could be easily collected. The receiver phase offset could, however, be determined from meteorological data in a similar fashion as is done for Z_{dr} calibration. The mean canting angles of ice particles in the ice phase of convective storms should on average be zero due to tumbling (the same assumption is used in practice to calibrate Z_{dr}). The mean canting angle can be determined from eigenpolarization analysis of the covariance matrix (Tragl 1990). Since the mean canting is quite sensitive to the co-to-cross phases $\arg\{\rho_{xH}\}$ and $\arg\{\rho_{xV}\}$, the unknown phase offset term can be adjusted until the mean canting in the ice phase is zero on average. The topics of determining system polarization errors and mean and standard deviation of canting angles from analysis of covariance matrix data will appear in Part II (Hubbert and Bringi 2003) and Part III of this paper.

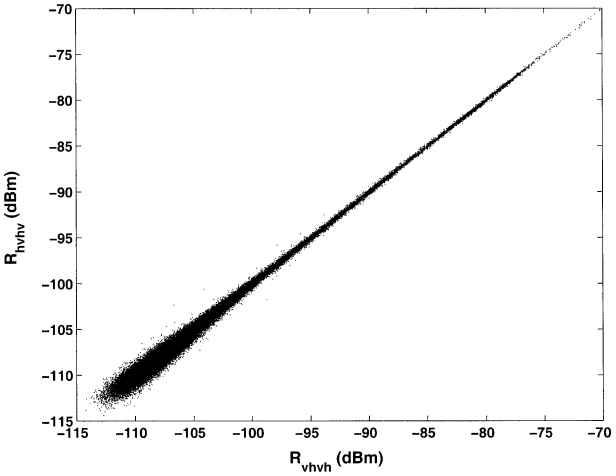

FIG. 4. Typical scatterplot of the two crosspolar powers from precipitation data from the CSU–CHILL radar.

c. An alternate LDR estimator

Another reason to record both cross-to-cross covariances is that they provide an alternate method for calculating LDR that is unbiased by noise in low SNR regions. The standard estimators of LDR, which employ the covariances $\langle \mathrm{HV}_i \mathrm{HV}_i^* \rangle$ and $\langle \mathrm{VH}_i \mathrm{VH}_i^* \rangle$, are biased by noise since the white noise is completely additive to the signal. Mathematically,

$$\langle \mathrm{HV}_i \mathrm{HV}_i^* \rangle = \langle \mathrm{HV}_i \mathrm{HV}_i^* \rangle_s + \sigma_n^2, \tag{40}$$

where $\langle \mathrm{HV}_i \mathrm{HV}_i^* \rangle_s$ is the signal portion and σ_n^2 is the noise portion of the covariance. This noise is typically estimated by pointing the radar at ''blue'' sky and measuring the received background noise, which is then subtracted from reflectivity estimates. However, the background white noise in HV_i and VH_i is uncorrelated because of the time lag between the two time series, so that

$$\langle \mathrm{HV}_i \mathrm{VH}_i^* \rangle = \langle \mathrm{HV}_i \mathrm{VH}_i^* \rangle_s. \tag{41}$$

This is similar to the pulse-pair estimate of mean Doppler velocity being unbiased by white noise. Thus, in low-SNR regions we suggest the following LDR_H estimator:

$$\mathrm{LDR}_{x,H}^m = \frac{|\langle \mathrm{HV}_i \mathrm{VH}_i^* \rangle|}{\langle \mathrm{HH}_i \mathrm{HH}_i^* \rangle \rho_{HH}(2)^{0.25}}, \tag{42}$$

where $\rho_{HH}(2)^{0.25} = \rho_{HH}(1)$ for Gaussian-shaped spectra, and $\rho_{HH}(2)$, $\rho_{HH}(1)$ are the first and second lag autocorrelations of the HH_i sequence. The correction term in the denominator is required because the HV_i and VH_i time series are not simultaneously sampled. This is the same correction factor used in calculating the copolar correlation coefficient [see (21)]. If the $\rho_{HH}(2) > 0.75$, the correction factor will only increase LDR by 0.31 dB. Thus, the correction factor represents a very small change in LDR, and even if this correction factor is poorly estimated, LDR should not be greatly affected. The LDR estimator of (42) also needs to be calibrated. Using similar analysis as was done for the CSU–CHILL system, it can be shown that

$$\mathrm{LDR}_{x,H} = \mathrm{LDR}_{x,H}^m \left(\mathcal{S}^2 \frac{R_{HVHV}}{R_{VHVH}} \right)^{0.5}. \tag{43}$$

3. Data analysis

The following data were gathered on 11 and 23 June 2000 during the STEPS experiment. Figure 4 is an example scatterplot of the two raw crosspolar powers, R_{VHVH} and R_{HVHV}, from precipitation. The scales are in decibels and the lower sensitivity limit of the radar is about −113 dBm. Figure 5 shows a plot of the statistics obtained by binning the horizontal axis into 3-dB steps and then averaging the data points that fall into these bins. The vertical lines represent a standard deviation on both sides of the mean (i.e., the vertical lines are 2σ long). The two small horizontal lines about each mean (barely visible) show the 95% confidence interval. As can be seen, the confidence intervals are quite small except perhaps for the last three bins ($R_{VHVH} > -75$ dBm), and thus the mean values should be quite accurate estimates of the actual receiver gain difference (including receive circulators) as a function of received power. To reveal the receiver gain difference as a function of input power, the receive power difference is plotted as a function of the mean value of R_{VHVH} denoted by $\overline{R_{VHVH}}$ in Figures 6a and 6b for the 11 and 23 June 2000 data, respectively. The three curves in each graph result from three separate volume scans with each set of three scans being gathered within a 20-min interval on their respective days. The curves are labeled with the start time of the volume scan. The sets of curves are in very close agreement, indicating the stability of the radar system [i.e., those components represented in (8) over such measurement time intervals]. The curves also re-

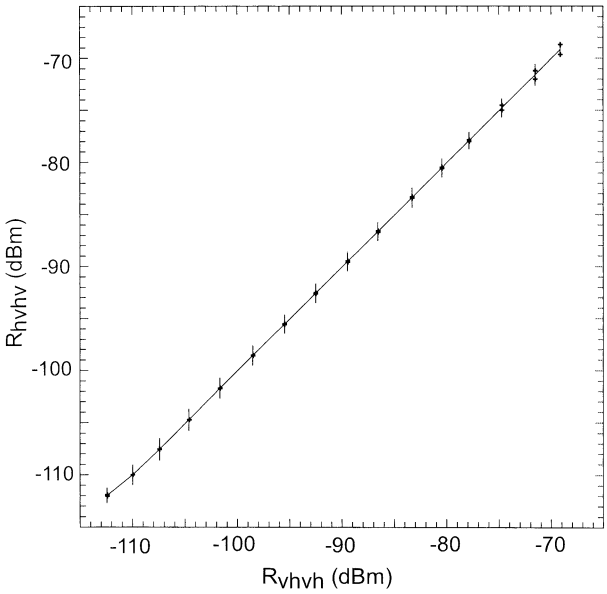

FIG. 5. Statistics for the scatterplot in Fig. 4. The 3-dB bins are used to calculate the mean. The line connects the mean values. Vertical lines through the mean points represent 2 std dev bars. The two small horizontal lines about the mean represent the 95% confidence interval.

veal a systematic variation of $\overline{R_{\mathrm{VHVH}}} - \overline{R_{\mathrm{HVHV}}}$ as a function of $\overline{R_{\mathrm{VHVH}}}$, and it will be shown below how to correct Z_{dr}^{m} for this systematic variation. The curves from 11 June vary by less than 0.1 dB, while the curves from 23 June vary by about 0.15 dB over the range of $\overline{R_{\mathrm{VHVH}}}$. Such variations are small but represent a significant error in Z_{dr} that should be corrected if possible. Examining (8), since the term $(P_{\mathrm{H}}C_{\mathrm{H}}^{T})/(P_{\mathrm{V}}C_{\mathrm{V}}^{T})$ should be constant (i.e., transmit power is assumed constant during a volume scan), the variation observed in Fig. 6 is due to radar system components represented by $(C_{\mathrm{V}}^{R}G_{\mathrm{V}}^{R})/(C_{\mathrm{H}}^{R}G_{\mathrm{H}}^{R})$, that is, the receivers and the receive circulators. To correct Z_{dr}^{m} for the variable bias seen in Fig. 6, both the crosspolar power ratio and the sun calibration are needed as functions of input power. Unfortunately, the sun calibration can only be done at one input power. However, notice that the term $(C_{\mathrm{V}}^{R}G_{\mathrm{V}}^{R})/(C_{\mathrm{H}}^{R}G_{\mathrm{H}}^{R})$ also appears in (3). The remaining terms in (3), $(W_{\mathrm{V}}G_{\mathrm{V}}^{A})/(W_{\mathrm{H}}G_{\mathrm{H}}^{A})$, are the antenna gains and the waveguide losses, both of which should not be a function of input power. Thus, the variable portions of (3) and (8) are identical, namely, $(C_{\mathrm{V}}^{R}G_{\mathrm{V}}^{R})/(C_{\mathrm{H}}^{R}G_{\mathrm{H}}^{R})$. The variability of this quantity as a function of input power is measured via a crosspolar power scatterplot, as shown in Fig. 6. Since the power level of input from the sun is known (typically around -100 dBm), the variability of $\mathcal{S}$ as a function of input power p can estimated from

$$\mathcal{S}(p) = \mathcal{S}_{\mathrm{ref}}\mathcal{X}(p)/\mathcal{X}_{\mathrm{ref}}, \tag{44}$$

where $\mathcal{S}(p)$ is the sun calibration figure as a function of measured received power, $\mathcal{S}_{\mathrm{ref}}$ is the actual measured sun calibration figure, $\mathcal{X}(p)$ is the average crosspolar

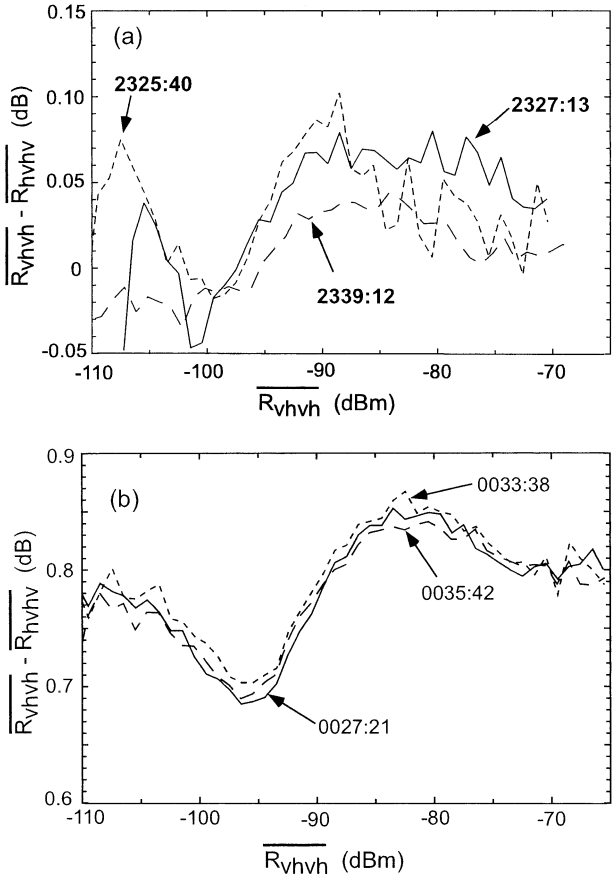

FIG. 6. Difference of the average of crosspolar powers (from 1-dB bins) vs the average crosspolar power $\overline{R_{\mathrm{VHVH}}}$. (a) 11 Jun and (b) 23 Jun data using the CSU–CHILL radar during STEPS. The times correspond to the beginning of the volume scan from which the curve is calculated.

power difference as a function of measured input power (Fig. 6), and $\mathcal{X}_{\mathrm{ref}}$ is the value of $\mathcal{X}(p)$ at the same measured power level of $\mathcal{S}_{\mathrm{ref}}$. Then Z_{dr} can be calibrated as a function of measured power using

$$Z_{\mathrm{dr}} = Z_{\mathrm{dr}}^{m}\mathcal{S}_{\mathrm{ref}}^{2}\mathcal{X}(p)/(\mathcal{X}_{\mathrm{ref}}^{2}). \tag{45}$$

For large Z_{dr}, p can be estimated by averaging R_{HHHH} and R_{VVVV}, the two copolar input powers.

This Z_{dr} correction method is now applied to an RHI volume scan from 11 June 2000 collected at 2327 UTC. Around this time a sun calibration was performed (at 2344 UTC) and vertical pointing data was also gathered (at 2328 UTC); thus, it is possible to compare the Z_{dr} correction method given by (45) and the vertical pointing data method. From the vertical pointing data the Z_{dr} bias is determined to be 1.3 dB. The sun calibration figure is 0.559 dB, and the sun power is about -100 dBm. The data in Fig. 6a (labeled 2327:13) are used with 3-dB bin intervals. Differential reflectivity Z_{dr} is corrected as a function of the received copolar horizontal power (R_{HHHH}). Figure 7 shows a vertical profile of Z_{H}, $Z_{\mathrm{dr}}^{\mathrm{vp}}$ (Z_{dr}^{m} corrected with vertical pointing data),

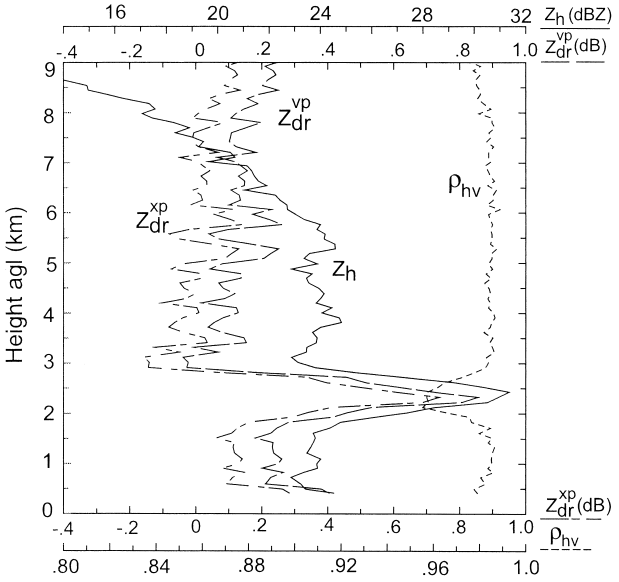

FIG. 7. Vertical profile of CSU–CHILL data from 11 Jun 2001 during STEPS.

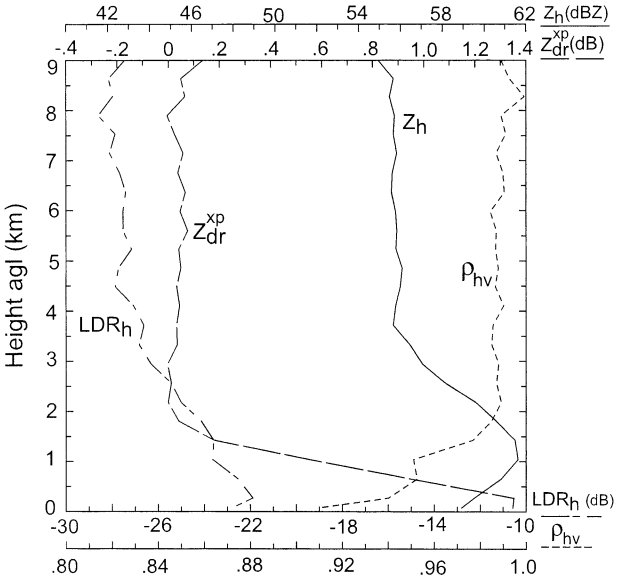

FIG. 8. Vertical profile of CSU–CHILL data from 23 Jun 2001 during STEPS.

Z_{dr}^{xp} (Z_{dr}^{m} corrected using the crosspolar power method), and $|\rho_{HV}|$. The data come from a trailing stratiform region of a convective cell and are averaged over a 5-km range (26–31 km). The Z_{dr}^{vp} and Z_{dr}^{xp} are offset by about 0.12 dB. It is impossible to say which one is more correct since the actual type, size, and orientation of the precipitation particles are unknown. At this altitude the precipitation particles are frozen and they often will be randomly distributed, thus making $Z_{dr} = 0$ dB. However, it is also frequently seen that Z_{dr} is positive (or negative) in stratiform regions or in storm anvils due to oriented pristine ice crystals (Caylor and Chandrasekar 1996; Bader et al. 1987). Thus it may be inaccurate to use the assumption of $Z_{dr} = 0$ dB in the ice phase to calibrate Z_{dr}. Furthermore, long periods of time frequently elapse with no precipitation over the radar, and thus vertically pointing data may not be available for Z_{dr} calibration. Using the difference of the crosspolar powers is an attractive, viable, and accurate way to calibrate Z_{dr}.

Figure 8 shows another vertical profile of data from 23 June 2001 through an intense convective core. No vertical pointing data was available that day. Data were averaged over a 5-km range (52–57 km). As can be seen, very high reflectivities (56 dBZ) are found through the upper level of the core. The Z_{dr}^{xp} is very slightly positive but is less than a tenth of a decibel from 2 to 9 km height. Since the convective core should be quite turbulent, ice particles are expected to be random in orientation distribution, and thus Z_{dr} should be 0 (dB). This example again shows that the crosspolar power method for calibrating Z_{dr} works well. For this case the received power levels were very high in the -55 to -65 dBm range. Figure 6b shows that the crosspolar power difference is only available up to -65 dBm, and thus correcting Z_{dr} at power levels greater than -65 dBm cannot be directly accomplished using crosspolar powers. However, by examining the calibration curves made on that day, the characteristics of the receivers and circulators at high power input levels can be observed. The receiver calibration curves for 23 June indicate that there was about a 0.05-dB decrease in receiver gain difference from about -75 dB to -55 dBm input power levels. This gain difference was incorporated into the Z_{dr} correction in Fig. 8.

The alternate LDR estimator

CSU–CHILL time series data from 24 June 2000 are used to illustrate the alternate LDR estimator in (42). The data are from from elevation angles greater than 4° at ranges 64–69 km and are therefore likely from a region of ice. Only light precipitation was present in the region between the radar and about 60 km, and thus the actual background noise present in the data will be close to the background noise of ''clear air'' [i.e., the noise temperature of ice and light rain is low; Gordon and Morgan (1993)]. Sun calibration data and ''clear air'' data were gathered immediately following the time series volume scan, so the calibrations for the time series dataset should be very accurate. The data are divided into low- and high-SNR categories. The threshold for the low-SNR data is -113 dBm $< R_{VHVH} < -110$ dBm and the threshold for the high-SNR data is $R_{VHVH} > -103$ dBm. A scatterplot of $LDR_{x,H}$ versus LDR_H for low-SNR data is shown in Fig. 9a. The LDR_H has been corrected for noise by subtracting the measured background noise (obtained from the clear air scan) from the measured crosspolar power. The two LDR estimators agree quite well considering the very low SNR. The statistics of the scatterplot are given in Fig. 9b, and it

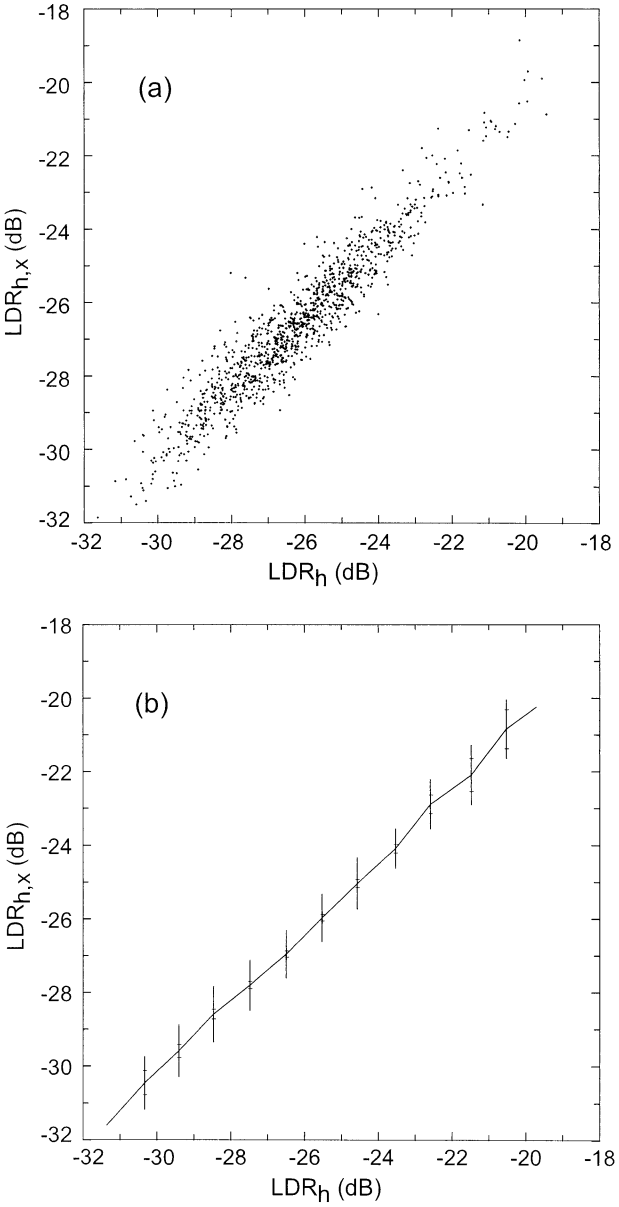

FIG. 9. (a) Scatterplot of $LDR_{x,H}$ vs LDR_H for cross powers of -113 dBm $< R_{HVHV} < -110$ dBm. (b) The mean value, std dev, and confidence intervals as described in Fig. 5. Data are from the CSU–CHILL radar.

can be seen that the $LDR_{x,H}$ estimator gives a slightly lower value on average by about a half a decibel. Similar plots are shown in Fig. 10 for the high-SNR case. The spread of the scatter is reduced considerably and the two LDR estimators are nearly identical on average, as expected, as seen in Fig. 10b. The $LDR_{x,H}$ estimate should actually be slightly lower than the standard LDR_H estimate since unpolarized energy will not be included in the $LDR_{x,H}$ estimate whereas it will be present in the standard LDR_H estimate.

Since accurate background noise estimates may not always be available, $LDR_{x,H}$ is an attractive alternate estimator. Furthermore, the background noise power is a function of the type and density of the precipitation medium intersected by the radar beam (Seminario et al. 2001; Gordon and Morgan 1993); that is, the noise power obtained from clear air measurements may not be indicative of the actual background noise for precipitation data. For example, a 50-dBZ echo region at 15 km can raise the noise floor by more than 2 dB when looking through the rain region (Seminario et al. 2001)! The $LDR_{x,H}$ estimator is immune to this problem.

4. Summary and conclusions

This paper gives a methodology to construct calibrated covariance matrices for both the CSU–CHILL radar and S-Pol configurations. The two radars are configured differently; that is, the CSU–CHILL uses two separate transmitters and two separate receivers (H receiver and V receiver), whereas S-Pol uses a single transmitter with a mechanical switch and two receivers (copolar receiver and crosspolar receiver via a transfer switch). A procedure for determining the two relative power calibration terms and three relative phase offsets was described. For S-Pol it was shown that the phase offsets for the co-to-cross covariances cannot be determined from precipitation data whereas they can be for the CSU–CHILL system. In order to determine the S-Pol phase offsets, external test horn measurements are required. Alternately, the co-to-cross covariance phase offsets can be determined from meteorological data by using the assumption that the mean canting angle of precipitation particles in the ice phase of convective storms is zero. It was also shown that for CSU–CHILL, the differential receiver power gain is a function of the input power level as shown by Fig. 6. Even though the amount of differential gain variation as a function of the input power is less than about 0.15 dB, this is significant when calculating Z_{dr}. To overcome this, a method was given to correct measured Z_{dr} for these differential receiver gain variations that utilize the crosspolar powers and sun calibration measurements. The differential receiver gain variation for the S-Pol configuration should be less than the CSU–CHILL receiver variation since all copolar signals are sent to the same receiver. To date, both CSU–CHILL and S-Pol Z_{dr} data have been calibrated either with vertical pointing data or with measurements in the ice phase of storms. Vertical pointing data are not always available, and indeed a Z_{dr} calibration method that relies upon rain over the radar site may not be reliable. The assumption that Z_{dr} is 0 (dB) in the ice phase of storms is also not always reliable, due to, for example, alignment of ice crystals or other anomalies in the radar data, such as reflectivity gradients, sidelobes, or three body scattering. Thus, the proposed Z_{dr} calibration technique is very attractive. It relies only on accurate sun calibrations and reciprocity of the crosspolar power measurements.

An alternate LDR estimator was also given that used

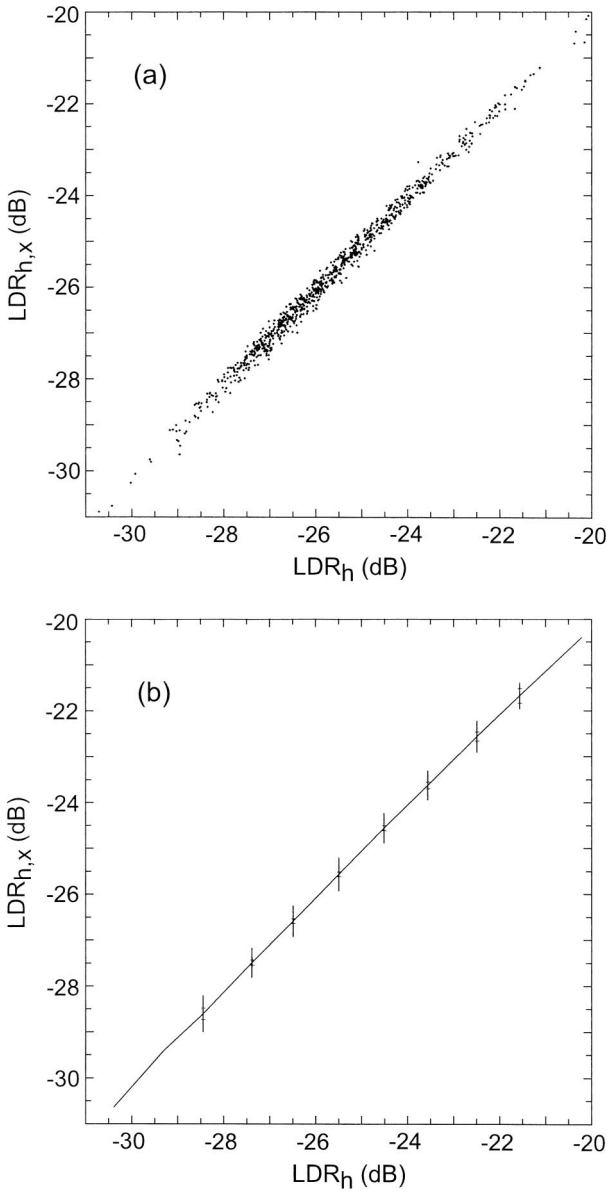

FIG. 10. Scatterplot of $LDR_{x,H}$ vs LDR_H for cross powers of $R_{HVHV} > -103$ dBm. (b) The mean value, std dev, and confidence intervals as described in Fig. 5.

the cross-to-cross covariances in contrast to using just the autocovariance of the crosspolar time series to calculate crosspolar power. The magnitude of the cross-to-cross covariance contains no background noise power since the white noise portion of the two crosspolar time series is uncorrelated. However, the magnitude of the cross-to-cross covariance is not a direct estimate of the crosspolar power, due to the time lag between the two time series. The amount of decorrelation due to this time lag can be estimated from the second lag correlation of the HH_i time series, $\rho_{HH}(2)$ (assuming Gaussian spectra), as is routinely done when estimating the copolar correlation coefficient. The LDR is typically corrected for noise by using background noise estimates obtained by pointing the radar at a precipitation-free region. However, it is known that this noise figure is also dependent on the precipitation that intersects the radar beam. Additionally, these noise measurements may not always be available. The new estimator, $LDR_{x,H}$, is immune to these effects. This new LDR estimator was applied to CSU–CHILL radar data and was shown to be in good agreement with the standard LDR_H estimator.

Acknowledgments. The CSU–CHILL radar is operated by Colorado State University via a cooperative agreement with the National Science Foundation (ATM-9500108). Two of the authors (JCH and VNB) were supported by this grant and NSF Grant ATM-9982030. The authors acknowledge the outstanding effort of Pat Kennedy and Robert Bowie in deploying and operating the radar for STEPS. The authors also acknowledge the technical discussions with Jon Lutz and Bob Rilling of the National Center for Atmospheric Research concerning S-Pol.

APPENDIX

S-Pol Sun Calibration Measurements

Because of the transfer switch in the receive path of S-Pol, four sun calibration measurements are required to completely characterize the system:

$$\mathrm{H}_{co} = G_{\mathrm{H}}^{A} W_{\mathrm{H}} C_{\mathrm{H}}^{R} \Gamma_{co,\mathrm{H}} G_{co}^{R}, \tag{A1}$$

$$\mathrm{V}_{co} = G_{\mathrm{V}}^{A} W_{\mathrm{V}} C_{\mathrm{V}}^{R} \Gamma_{co,\mathrm{V}} G_{co}^{R}, \tag{A2}$$

$$\mathrm{H}_{x} = G_{\mathrm{H}}^{A} W_{\mathrm{H}} C_{\mathrm{H}}^{R} \Gamma_{x,\mathrm{H}} G_{x}^{R}, \tag{A3}$$

$$\mathrm{V}_{x} = G_{\mathrm{V}}^{A} W_{\mathrm{V}} C_{\mathrm{V}}^{R} \Gamma_{x,\mathrm{V}} G_{x}^{R}, \tag{A4}$$

where Γ represents the attenuation through the various paths of the switch. For example, $\Gamma_{co,H}$ is the attenuation along the path beginning from the H input port of the switch to the input of the copolar receiver G_{co}^{R} (see Fig. 3). In order to calibrate LDR_H^m and Z_{dr}^m, the three following ratios are needed:

$$\mathcal{S}_1 = \frac{\mathrm{V}_{co}}{\mathrm{H}_{co}} = \frac{G_{\mathrm{V}}^{A} W_{\mathrm{V}} C_{\mathrm{V}}^{R} \Gamma_{co,\mathrm{V}}}{G_{\mathrm{H}}^{A} W_{\mathrm{H}} C_{\mathrm{H}}^{R} \Gamma_{co,\mathrm{H}}}, \tag{A5}$$

$$\mathcal{S}_2 = \frac{\mathrm{V}_{x}}{\mathrm{H}_{x}} = \frac{G_{\mathrm{V}}^{A} W_{\mathrm{V}} C_{\mathrm{V}}^{R} \Gamma_{x,\mathrm{V}}}{G_{\mathrm{H}}^{A} W_{\mathrm{H}} C_{\mathrm{H}}^{R} \Gamma_{x,\mathrm{H}}}, \tag{A6}$$

$$\mathcal{S}_3 = \frac{\mathrm{V}_{x}}{\mathrm{H}_{co}} = \frac{G_{\mathrm{V}}^{A} W_{\mathrm{V}} C_{\mathrm{V}}^{R} \Gamma_{x,\mathrm{V}} G_{x}^{R}}{G_{\mathrm{H}}^{A} W_{\mathrm{H}} C_{\mathrm{H}}^{R} \Gamma_{co,\mathrm{H}} G_{co}^{R}}. \tag{A7}$$

These ratios are used in (28) and (29).

REFERENCES

Bader, M. J., S. A. Clough, and G. P. Cox, 1987: Aircraft and dual polarization radar observations of hydrometeors in light stratiform precipitation. *Quart. J. Roy. Meteor. Soc.*, **113,** 491–515.

Bringi, V. N., and V. Chandrasekar, 2001: *Polarimetric Doppler Weather Radar*. Cambridge University Press, 636 pp.

Brunkow, D. A., 1999: A new receiver and signal processor for the CSU–CHILL radar. Preprints, *29th Int. Conf. on Radar Meteorology*, Montreal, QC, Canada, Amer. Meteor. Soc., 256–258.

——, V. N. Bringi, P. C. Kennedy, S. A. Rutledge, V. Chandrasekar, E. A. Mueller, and R. K. Bowie, 2000: A description of the CSU–CHILL National Radar Facility. *J. Atmos. Oceanic Technol.,* **17,** 1596–1608.

Caylor, I. J., and V. Chandrasekar, 1996: Time-varying ice crystal orientation in thunderstorms observed with multiparameter radar. *IEEE Trans. Geosci. Remote Sens.*, **34,** 847–858.

Gordon, G. D., and W. L. Morgan, 1993: *Principles of Communications Satellites*. John Wiley and Sons, 533 pp.

Gorgucci, E., G. Scarchilli, and V. Chandrasekar, 1999: A procedure to calibrate multiparameter weather radar data using the properties of the rain medium. *IEEE Trans. Geosci. Remote Sens.*, **17,** 269–276.

Huang, G. J., J. C. Hubbert, and V. Bringi, 2001: Precipitation canting angle distribution estimates from covariance matix analysis of CSU–CHILL radar data. Preprints, *30th Int. Conf. on Radar Meteorology*, Munich, Germany, Amer. Meteor. Soc., 651–653.

Hubbert, J., and V. N. Bringi, 1995: An iterative filtering technique for the analysis of copolar differential phase and dual-frequency radar measurements. *J. Atmos. Oceanic Technol.*, **12,** 643–648.

——, and ——, 2001: Estimation of polarization errors from covariance matrices of CSU–CHILL radar data. Preprints, *30th Int. Conf. on Radar Meteorology*, Munich, Germany, Amer. Meteor. Soc., 45–47.

——, and ——, 2003: Studies of the polarimetric covariance matrix. Part II: Modeling and polarization errors.. *J. Atmos. Oceanic Technol.*, in press.

——, ——, and G. Huang, 1999: Construction and interpretation of S-band covariance matrices. Preprints, *29th Int. Conf. on Radar Meteorology*, Montreal, Canada, Amer. Meteor. Soc., 205–207.

Jameson, A. R., 1985: Microphysical interpretation of multi-parameter radar measurements in rain. Part III: Interpretation and measurement of propagation differential phase shift between orthogonal linear polarizations. *J. Atmos. Sci.*, **42,** 607–614.

Keeler, R. J., J. Lutz, and J. Vivekanandan, 2000: S-POL: NCAR's polarimetric Doppler research radar. Preprints, *IGARSS-2000*, Honolulu, HI, IEEE, 1570–1573.

Mueller, E. A., 1984: Calculation procedures for differential propagation phase shift. Preprints, *22d Conf. on Radar Meteorology*, Zürich, Switzerland, Amer. Meteor. Soc., 397–399.

Ryzhkov, A. V., 2001: Interpretation of polarimetric radar covariance matrix for meteorological scatterers: Theoretical analysis. *J. Atmos. Oceanic Technol.*, **18,** 315–328.

Sachidananda, M., and D. S. Zrnić, 1986: Differential propagation phase shift and rainfall rate estimation. *Radio Sci.*, **21,** 235–247.

Saxon, D. S., 1955: Tensor scattering matrix for the electromagnetic field. *Phys. Rev.*, **100,** 1771–1775.

Seminario, M., K. Gojara, and V. Chandrasekar, 2001: Noise correction of polarimetric radar measurements. Preprints, *30th Int. Conf. on Radar Meteorology*, Munich, Germany, Amer. Meteor. Soc., 38–40.

Tragl, K., 1990: Polarimetric radar backscattering from reciprocal random targets. *IEEE Trans. Geosci. Remote Sens.*, **8,** 856–864.